Journal of Chromatography A, 1216 (2009) 5511–5517

Contents lists available at ScienceDirect

Journal of Chromatography A

journal homepage: www.elsevier.com/locate/chroma

# Visualization and quantification of the onset and the extent of viscous fingering in micro-pillar array columns

Wim De Malsche[a,*], Jeff Op De Beeck[a], Han Gardeniers[b], Gert Desmet[a]

[a] Department of Chemical Engineering, Vrije Universiteit Brussel, Pleinlaan 2, B-1050 Brussels, Belgium
[b] Research Programme Mesofluidics, MESA+ Institute for Nanotechnology, P.O. Box 217, 7500 AE Enschede, The Netherlands

ARTICLE INFO

*Article history:*
Received 6 March 2009
Received in revised form 20 April 2009
Accepted 24 April 2009
Available online 3 June 2009

*Keywords:*
Viscous fingering
Microfluidics
Size exclusion chromatography
Lab-on-a-chip
Pillar array column
Collocated monolithic support structure
Band broadening source

ABSTRACT

New experimental data of the viscous fingering (VF) process have been generated by studying the VF process in perfectly ordered pillar array columns instead of in the traditionally employed packed bed columns. A detailed quantitative analysis of the contribution of VF to the observed band broadening could be made by following the injected species bands using a fluorescence microscope equipped with a CCD-camera. For a viscosity contrast of 0.16 cP, a plate height increase of about 1 μm can be observed, while for a contrast of respectively 0.5 cP and 1 cP, additional plate height contributions of the order of 5–20 μm were observed. Citing these values is however futile without noting that they also depend extremely strongly on the injection volume of injected sample. It was found that, for a given viscosity contrast of 0.314 cP, the maximal plate height increase varied between 0.5 μm and 18 μm if the injection volume was varied between 3.0 nl and 32.7 nl. These values furthermore also strongly vary with the distance along the column axis.



## 1. Introduction

It is known for many years that the injection of sample plugs having a different composition than the mobile phase can result in severe peak disturbance. In size exclusion chromatography (SEC), it has been recognized since 1976 [1] that viscosity mismatches may result in Saffman–Taylor instabilities [2], which are nowadays referred to as viscous fingering (VF) [3–7]. In reversed-phase HPLC, where the observed performance losses were most often explained due to differences in solvent strength, the effect of VF was ignored completely for a very long time [8–10]. Nowadays, however, the occurrence of VF is generally accepted as a potential source of band broadening [9–14]. Viscosity mismatches for example occur when insufficient efforts are made to restore a liquid sample into the same solution as that used as the mobile phase. Another example can be encountered in multi-dimensional separations, where it is very common that the mobile phase of the first dimension is completely different from the mobile phase of another dimension. Another situation where the viscosity difference can be considerable when the sample contains macromolecular components in high concentrations [15,16].

In the early literature, magnetic resonance imaging was used to visualise VF in packed beds [17]. Even though very informative, this technique requires additives (preventing to work in realistic conditions) to visualise the fluid flow and has a low spatial resolution (1 $mm^3$) [18]. Later on, Catchpoole et al. [19] used filled glass columns with particles and tuned the mobile phase such that the refractive index was identical to that of the particles, in this way rendering the column transparent and allowing to make optical images of the column interior.

A lot of theoretical work [2,20–23,4,6] has been performed on the stability and behaviour of fronts between two liquids that have differing viscosities. This work is mostly based on linear stability analysis, in which small periodic perturbations are imposed on the front surface, which allows the determination of a most probable characteristic finger wavelength and an onset time. Numerical simulations on finite slices have been performed as well. This approach allowed for a very good prediction of the expected trends, but, as is the case in linear stability analysis, this method is depending on a predefined noise level [24,6].

The impact of VF on column performance has been a topic of debate the last couple of years. The discussion about the importance of VF as a peak distorting effect is partly caused by the following. When a plug resides sufficiently long in a column, dispersive effects other than VF continuously dilute the sample and finally remove the viscosity contrast (and hence VF) completely. At this stage, the plug acquires a Gaussian shape, many times broader however than

* Corresponding author. Tel.: +32 2 629 37 81; fax: +32 2 629 32 48.
*E-mail address:* wdemalsc@vub.ac.be (W. De Malsche).

0021-9673/$ – see front matter © 2009 Elsevier B.V. All rights reserved.
doi:10.1016/j.chroma.2009.04.098

under non-VF conditions. To explain this abnormally broad peak, the analyst will then usually look for explanations other than VF, because VF is usually associated with the observation of severely distorted peak shapes. A moderating remark here is that it can be predicted that the impact of VF looses importance with increasing retention [25]. When analytes reside most of their time on the stationary phase, the original dissolution medium will overtake the retained plug and leave the molested plug behind in the column to move at its pace to recover faster from its disturbance.

For conventional HPLC columns, it is generally assumed that the VF effect is negligible when the viscosity contrast is smaller than 0.15 cp [26]. The experiments leading to these conclusions were however conducted in columns that were typically 250 mm long, where the VF-induced dispersive effects are less visible than in shorter columns.

The present study has been initiated to generate new experimental data that can be of use for the ongoing theoretical work on the subject [24,25,6]. The data are new because they have been obtained in perfectly ordered beds, fabricated using micromachining technologies [27,28], and consisting of an array of uniformly sized and positioned cylindrical micro-pillars. These micro-pillar beds have a flat rectangular cross-section and can hence be viewed as a pillar containing analogue of the Hele–Shaw cell [21]. Being formed as a sandwich of a silicon and a (transparent) Pyrex substrate, these micro-pillar arrays are also ideally suited for visualization purposes, without the need for mobile phase adjustments to enable optical density matching. The channels also offer a maximal imaging resolution, as the microscope objective can be placed directly above the entire channel, without having to compromise for the focus as is the case in cylindrical tubes.

In order to exclude retention-based dispersion effects and its predicted complex interaction with VF [6,25], the present study has been conducted under non-retained conditions.

## 2. Experimental

### 2.1. Channel fabrication

The pillar array consisted of a 3 cm long and 1 mm wide channel in which cylindrical pillars with a diameter of 5 μm are equilaterally positioned at an inter-pillar distance of 2.5 μm, as it was patterned on the photolithographic mask. The pillar channels were defined in a silicon–glass sandwich. First, a 100 mm diameter (1 0 0) silicon wafer (p-type, 5–10 Ω cm resistivity) was thermally (dry) oxidized at 1100 °C until 200 nm silicon oxide was formed (Amtech Tempress Omega Junior). Then, normal UV photolithography (photoresist: Olin 907-12) was used to define the pillar array. Subsequently, the exposed silicon oxide was dry etched (Adixen AMS100DE), after which the resist was removed by oxygen plasma and nitric acid. Another lithography step was then used to define the inlet and outlet channels. The exposed silicon oxide was then etched and a Bosch-type deep reactive ion etch (Adixen AMS100SE) was used to make these channels 60 μm deep. After stripping the resist, another 12 μm was Bosch-etched into the exposed silicon, leaving pillars of 12 μm height and supply channels with a total depth of 72 μm. The top of the channels was formed by a 100 mm diameter Pyrex® wafer (thickness 0.5 mm). On the silicon wafer, through-holes were first defined by photolithography on a dry resist foil (Ordyl BF410). The exposed glass was subsequently powder blasted using 30 μm alumina particles. After stripping the foil, the substrates were anodically bonded (voltage ramped to a maximum of 1000 V at 400 °C, on an EVG EV-501 wafer bonder).

### 2.2. System hardware and injection procedures

The injection occurred on-chip as described previously [27,28]. In short, pressurized vessels, controlled by two pressure controllers, were used to provide the required pressure for the flow generation in the two steps of the injection process. The sample reservoir as well as the mobile phase reservoir consisted of two different home-made stainless steel vessels coupled to 0.2 μm pore size filters. The vessels were independently connected to two different pressure controllers (Bronkhorst, The Netherlands), fed by a nitrogen gas bottle, that allowed to control the pressure in the vessels with a millibar precision. This approach allowed applying two different independent pressure settings, one for the sample injection and one for the mobile phase flow. The plug was formed in situ just before the area where the pillar channel starts. Prior to the 1 mm wide pillar channel, a flow distributor region containing transversally oriented diamond shaped pillars was etched to distribute the liquid coming from the supply channel (10 μm width) evenly across the actual cylinder bed [29].

### 2.3. Dispersion experiments

The different viscosity contrasts needed to study the VF effects were obtained by ranging the mobile phase (mp) from 0% (v/v) to 50% (v/v) water/methanol while holding the sample (s) composition (1 mM coumarin 480, Cas no. 41267-76-9, dissolved in HPLC-grade methanol, Across Organics, Belgium) constant. The corresponding viscosity contrasts ($\Delta\nu = \nu_{mp} - \nu_s$, with $\nu_{mp}$ the mobile phase viscosity and $\nu_s$ the sample viscosity) were calculated according to Li and Carr [30], these are listed in Table 1 for a working temperature of 20 °C. Several viscosity correlations are available in the literature but all give similar values [31]. Using a sample consisting of pure methanol allowed to keep the C480 coumarin dye in the sample well dissolved (C480 does not dissolve in water). All experiments were conducted at a mobile phase velocity of 2 mm/s. Most of the experiments were carried out for a positive $\Delta\nu$, a situation for which the fingering effect takes place at the downstream part of the sample plug instead of at the upstream part.

To study the influence of the injection volume on the extent of VF, peak volumes were varied between 3.0 nl and 32.7 nl. Plate heights were determined by using a single line of pixels (width = 10 μm) across the hole width of the channel as a monitor line at several positions downstream the channel and by subsequently applying the method of moments on the chromatograms recorded at these monitor lines, using:

$$H = \frac{u^2 \Delta\sigma_t^2}{l} \quad (1)$$

wherein $\Delta\sigma_t^2$ is the difference between the time-based variance of the peak at a position $x = l$ and that at position $x = 0$ (bed entrance), and wherein $u$ is the mean liquid velocity.

**Table 1**
Viscosity contrast values, absolute viscosity values and viscosity ratios [30] for the different methanol–water mixtures used as the mobile phase in the present study ($\nu_s$ = sample viscosity, $\nu_{mp}$ = mobile phase viscosity, $\Delta\nu$ =), the sample viscosity is 0.600 cP.

| $V_{H_2O}$ (%) | 0 | 0.5 | 1.0 | 1.5 | 2.0 | 2.5 | 5.0 | 7.5 | 10.0 | 20.0 | 30.0 | 40.0 | 50.0 |
|---|---|---|---|---|---|---|---|---|---|---|---|---|---|
| $\nu_{mp}$ (cP) | 0.600 | 0.617 | 0.634 | 0.651 | 0.668 | 0.684 | 0.764 | 0.841 | 0.914 | 1.173 | 1.379 | 1.534 | 1.636 |
| $\Delta\nu$ (cP) | 0 | 0.017 | 0.034 | 0.051 | 0.068 | 0.084 | 0.164 | 0.241 | 0.314 | 0.573 | 0.779 | 0.934 | 1.360 |
| $\nu_{mp}/\nu_s$ | 1 | 1.03 | 1.06 | 1.09 | 1.11 | 1.14 | 1.27 | 1.40 | 1.52 | 1.96 | 2.30 | 2.56 | 2.73 |

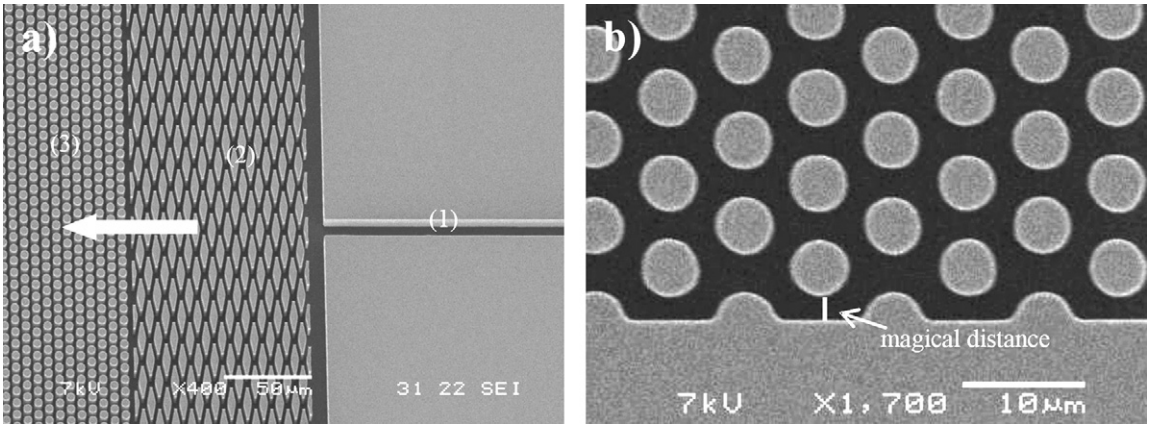


**Fig. 1.** SEM pictures of (a) the top section of the pillar array column, where the sample and the mobile phase (flow direction indicated by arrow) enter the bed through a 10 μm wide connection channel (1), then passes over the flow distributor zone (2) before entering the 1 mm wide bed (3) of cylindrical pillars with an inter-pillar distance of 2.5 μm and (b) the side-wall region of the pillar array, consisting of a series of embedded semi-circular cylinders positioned at a "magical distance" of 1.8 μm to avoid severe side-wall induced band broadening [27].

The detection set-up consisted of a Hg-vapor lamp (U-LH100HGAPO, Olympus, Belgium) to excite the fluorescent coumarin dyes in the UV region and an inverted microscope (IX71, Olympus, Belgium) equipped with an UV-1 filter cube set (UV-2A DM400 Nikon, Cetec N.V., Belgium) to collect the emitted light. The microscope was mounted on a breadboard (M-IG 23–2, Newport, The Netherlands), together with a linear displacement stage (M-TS100DC) and a speed controller (MM, 4006 Newport) used to displace the channels opposite to the movement of the sample plugs, so as to keep these sample plugs at rest with respect to the microscope objective. The separations were visualised using a CCD fluorescent camera (ORCA-ER4742, Hamamatsu Photonics, Belgium) mounted on the video adapter of the microscope and analyzed with the accompanying SimplePCI 6 software.

## 3. Results and discussion

Fig. 1 shows SEM pictures of the employed micro-pillar array channel. Fig. 1a emphasizes the fact that the channels were preceded by a flow distributor, mimicking the flow distributing effect of the so-called column "frits" heading conventional packed bed columns and spreading the injected sample and the mobile phase entering the bed via a narrow connection channel as uniformly as possible across the cross-section of the cylinder bed acting as the actual separation column.

Fig. 1b shows a detail of the side-wall region of the cylindrical pillar bed, on the one hand showing the high uniformity of the produced pillar array, and on the other hand showing the actual design of the pillar bed near the side-wall, as well as the specific distance (so-called "magical wall distance") that was imposed between the semi-cylindrical pillars embedded in the side-wall and the first row of full pillars. This magical distance is needed to ensure that the flow resistance in the side-wall region of the bed is equal to that in the remainder of the bed, hence preventing the formation of a preferential flow-path. Guided by computational fluid dynamics simulations [29,32], the magical distance (as indicated by the arrow) was set at 1.8 μm for the present case. During the fabrication, this distance should be respected as close as possible (despite the potential errors evolving from the inevitable underetching [27]), for otherwise a significant velocity difference will develop between the side-wall zone and the central portion of the bed, giving rise to a significant extra plate height contribution [33]. The use of channels without a noticeable side-wall effect is also very important to study VF effects. This became apparent during our first separation experiments conducted on a crudely designed chip having a non-optimized distance between the nearest pillar to the channel wall and the wall itself. Not only did this side-wall effect lead to a plate height contribution that was already as large as a few tens of micrometers, tending to overshadow the VF effects, the difference in flow resistance also clearly favoured the formation of viscous fingers in the wall zone. As a consequence, we were studying a system with a predestined location of the finger formation, and the results of this study would certainly have been biased by this fact. In the presently employed chips, the side-wall region distance was fully optimized, so that no significant lateral flow resistance difference was induced.

Before starting with the actual VF experiments, the fabricated pillar array was characterized by measuring the band broadening in the absence of VF. For this purpose, a van Deemter curve was measured in pure methanol (see Fig. 2), yielding a minimal plate height of the order of 2.5 μm. This value is in fair agreement with earlier non-retained species experiments conducted in pillar array columns [27] where minimal plate height values of the order of 1.5 μm were obtained in pillar beds with an inter-pillar distance of 1.7 μm. In order to limit the variables in this exploratory work concerning VF in pillar array column, all subsequent experiments have been conducted at a mobile phase velocity of 2 mm/s (corresponding to the optimal velocity of the van Deemter curve), although we realize that the mobile phase velocity certainly also has an impact on the observed VF behaviour [6].

Fig. 3 shows a compilation of the recorded VF patterns as a function of the viscosity contrast and the position in the channel. In the top row of images, both the sample and the mobile phase are composed of pure methanol, representing the case of a zero vis-

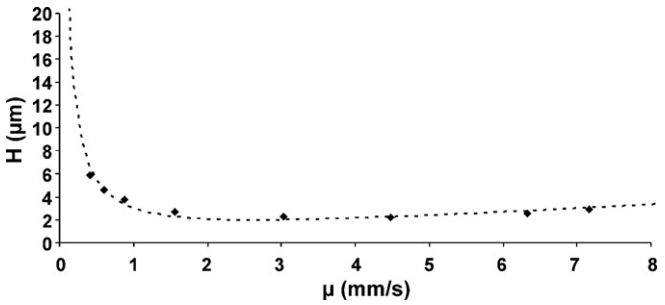


**Fig. 2.** van Deemter plot of coumarin C480 (1 mM) in MeOH. The dashed line depicts the best fit with the van Deemter equation ($H = A + B/u + Cu$, with $A = 0$, $B = 2.7 \times 10^{-9}$ m$^2$/s, $C = 3.8 \times 10^{-4}$ s).

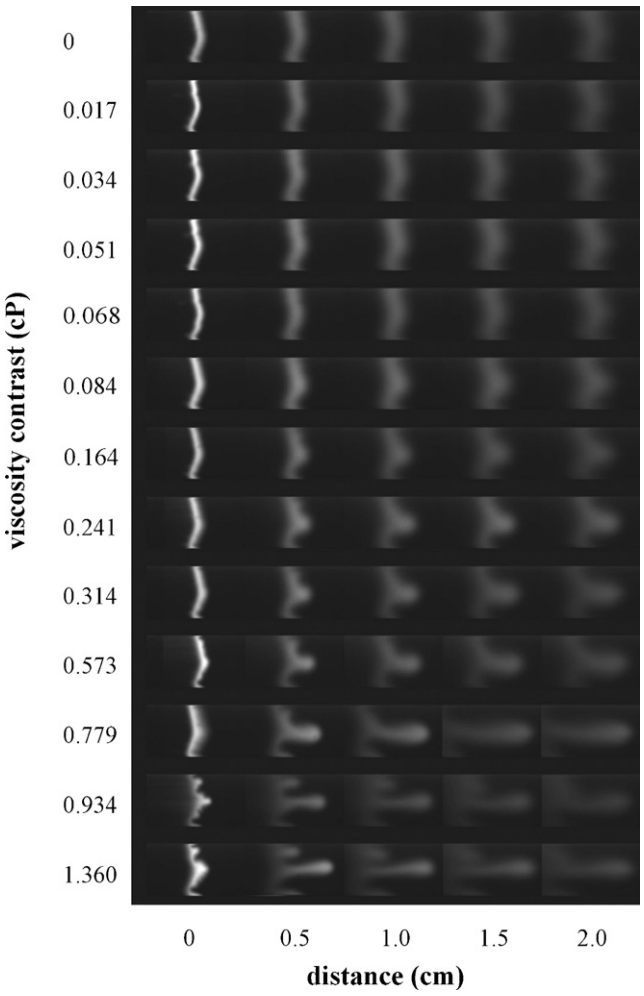


**Fig. 3.** Visualization of coumarin dye plugs dissolved in pure methanol travelling through the pillar array from left to right at a mobile phase velocity of 2 mm/s. Pictures taken at the injection zone (0 cm), and subsequently at a position 0.5 cm, 1.0 cm, 1.5 cm and 2.0 cm downstream of the inlet. The corresponding viscosity contrasts are shown on the *y*-axis of the figure and range from 0 cP to 1.360 cP.

cosity contrast. It can be noted that even under these conditions the band is not perfectly straight when it enters the bed. This is however solely due to the imperfect functioning of the frit (which might in fact also be the case in real packed columns), and has no further impact on the obtained results, for the plate heights that were measured from these slightly warped bands did not vary with the position in the column (see below), and were close to the theoretical expectations based on CFD simulations and previous experiments [27,34]. Subsequently considering the lower rows of CCD camera images shows that first a small additional broadening can be observed at the 2 cm point as soon as the viscosity contrast reaches some 0.05–0.07 cP. From 0.08 cP on, a significant peak shape change (appearance of a central bulb) is also visible in the video frame recorded at 0.5 cm. This disturbance grows further downstream into a slightly bigger bulb. For a viscosity contrast of the order of 0.2–0.3 cP, the elongated "fingers" that are so typical for the VF phenomenon are being formed. Interesting to note is also that these fingers (as well as the initial bulb) are always formed at the very center of the channel (see Fig. 8 further on to appreciate the repeatability of the finger formation). Visual inspection of the SEM pictures allowed to rule out that this preferential formation position is caused by some local bed defects. Another possible explanation for the preferred finger formation location could be the warped shape of the band as it enters the bed, but we are more inclined to see the central formation position as a mere consequence of the symmetry of the system [2]. This is further corroborated by the fact that at even higher viscosity contrasts (order of 0.8 cP and more), two side-fingers are being formed, symmetrically positioned with respect to the central finger.

In parallel with the picture analysis, the CCD camera images were also analyzed in time space, recording the fluorescence intensity at a given monitor line as a function of the time. Since our set-up allowed doing this at different successive positions along the channel axis, detailed information about the evolution of the peak shape with time could be obtained. Fig. 4a for example shows how, at a fairly large viscosity contrast of 0.578 cP, the injected band slowly deforms from a single peak into a two-bumped peak. Theoretical expectations [24] show that at further positions downstream the channel, even more bumps would develop, eventually leading to a broadly smeared band. Fig. 4b illustrates the effect of the viscosity contrast on the peak shape, recorded at a given distance (1 cm) away from the bed inlet. Obviously, an increased viscosity contrast leads to a transition from a single- to a two-bumped peak, with the bumps becoming most pronounced at the highest viscosity contrast.

To discuss the VF effects observed in Fig. 3 on a quantitative basis, Fig. 5 shows the corresponding plate height values obtained by applying Eq. (1) to the peak profiles recorded at the various positions inside the channel (see e.g., Fig. 4a). The measurements for 0.017 cP, 0.034 cP, 0.051 cP and 0.068 cP viscosity contrast have been omitted because they are nearly coincident with the zero contrast case.

Whereas the data points for the 0.084 cP viscosity contrast still coincide within the error margins with the zero viscosity contrast case, the data points for the 0.164 cp viscosity contrast already lie significantly higher (about 1 μm). This allows to conclude that from this point on the VF starts to have a noticeable effect. However, given the small difference with the zero contrast case, and given the fact that also the 0.084-cP data appear to lie somewhat higher in the first few data points (hence reflecting the appearance of the central "bulb" in the 0.084-cP case already observed when discussing Fig. 3), it can be inferred that the onset of VF does not require a certain viscosity contrast threshold to be surpassed. Instead, the VF process appears as a steadily growing source of additional band broadening, coming into effect as soon as the viscosity of the sample and that of the mobile phase become different. Of course, the viscosity difference needs to be sufficiently large before the VF effect becomes measurable. The apparent absence of a threshold is also in line with the early theoretical analysis of the VF phenomenon of Saffman [2], showing that the interface between two regions with different viscosity becomes unstable to small disturbances from the smallest possible difference in viscosity on. Fig. 5 also shows that, as soon as the viscosity contrast exceeds 0.5 cP, an extremely large additional band broadening effect can be expected, yielding excess plate height values of the order of some 5–20 μm.

Another interesting feature of Fig. 5 is that the plate heights in the high viscosity contrast cases all display a steep initial increase, reaching their maximum somewhere downstream the bed followed by a subsequent slow decrease of the effect. The latter is believed to be caused by a reduction of the viscosity contrast caused by the inevitable dilution of the finite sample plug [24].

Another important observation is that any quantitative interpretation of VF should not only be made in relation to the viscosity contrast, but also to the amount of injected material. Knowing from Fig. 5 that the dilution experienced by the sample plug as it moves through the column leads to a moderation of the VF-induced band broadening, it is also straightforward to expect that, since low volume peaks dilute much faster than large volume peaks, the former will display a stronger VF effect than the latter. This is exactly what is observed in Fig. 6, where the viscosity contrast is kept constant (at a value of 0.314 cP) while the injection volume

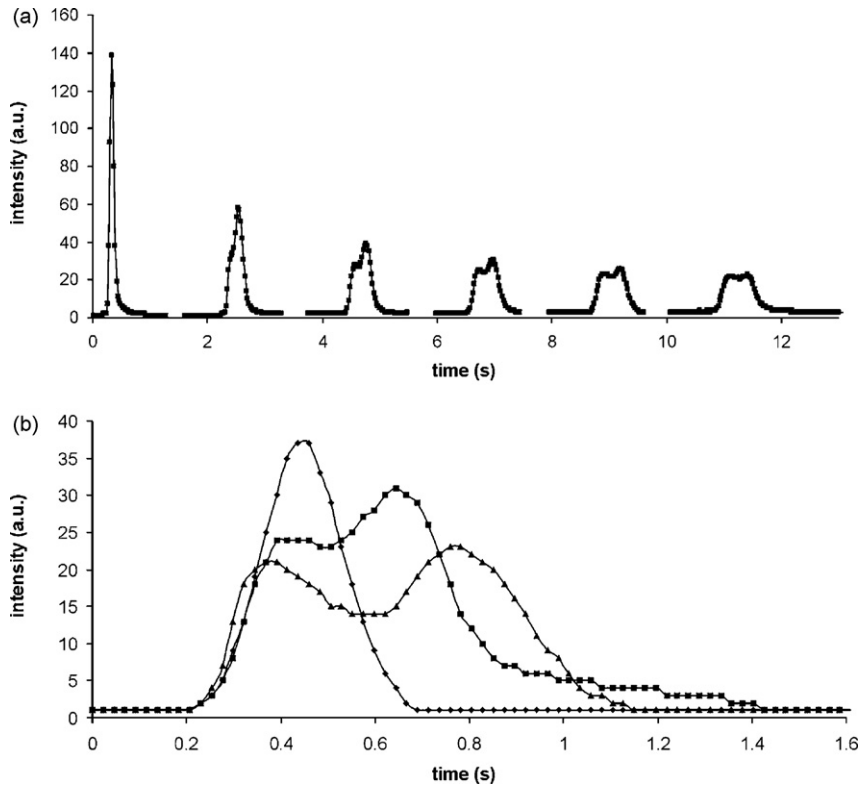


**Fig. 4.** (a) Successive fluorescence intensity readouts of a migrating solute band (C480) dissolved in pure methanol and using a mobile phase with a 0.573 cP viscosity contrast and recorded at different positions along the channel axis at 0.5 cm intervals. (b) Readouts of a migrating solute band (C480) dissolved in pure methanol, recorded at 1 cm downstream of the bed inlet and for three different viscosity contrasts, i.e., 0 cP (—◆—), 0.573 cP (—■—) and 1.360 cP (—▲—).

is varied. The corresponding plate height values are represented in Fig. 7. As can be noted, the effect of the injection volume is striking, with a VF contribution to the observed plate height values ranging from about 0.5 μm to 1 μm (at the positions closest to the bed inlet) for the 3.0 nl injection to about 18 μm for the 32.7 nl injection, as is the case without VF. For larger band widths however, contributions of up to 18 μm were reached. An interesting point to be noted here is that the initial formation of the finger now no longer proceeds symmetrically. SEM inspection of the bed could not reveal any particular spot in the bed that would induce the observed specific form. Our current hypothesis is that small differences in permeability of the inlet distributor (possibly induced by the presence of small solid particles or air bubbles) lie at the origin of this (highly repeatable) asymmetrical pattern. Interesting to note is that, despite its asymmetric onset, the finger afterwards transits into a perfectly symmetric finger. From 1.5 cm

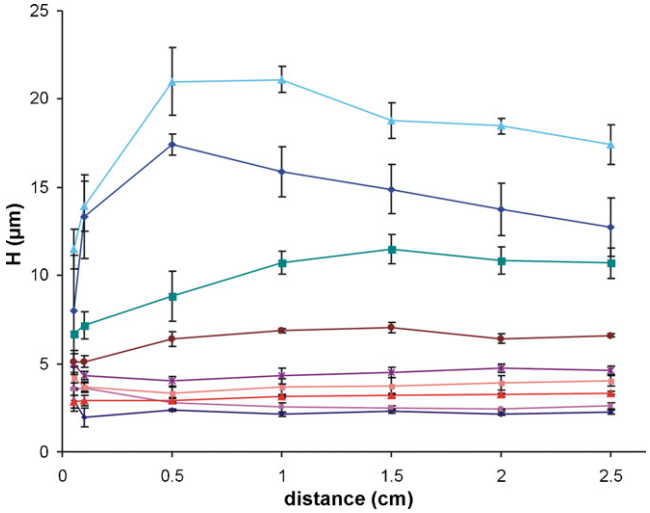


**Fig. 5.** Evolution of the plate height of coumarin C480 as a function of the elapsed distance in the channel for different mobile phase compositions at a mobile phase velocity of 2 mm/s and a viscosity contrast of 0 cP (—◆—), 0.084 cP (—●—), 0.164 cP (—▲—), 0.241 cP (—■—), 0.314 cP(—✱—), 0.573 cP (—●—), 0.779 cP (—■—), 0.934 cP (—◆—) and 1.036 cP (—▲—).

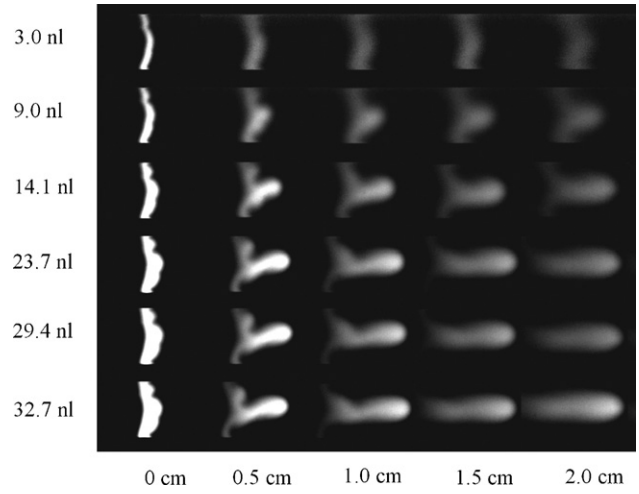


**Fig. 6.** Camera frames demonstrating the influence of increasing injection volumes (see *y*-axis values) on the dispersion behaviour for the case of a viscosity contrast of 0.314 cP and a mobile phase velocity of $u = 2$ mm/s. Images taken at different positions downstream of the bed inlet (with 0.5 cm intervals).

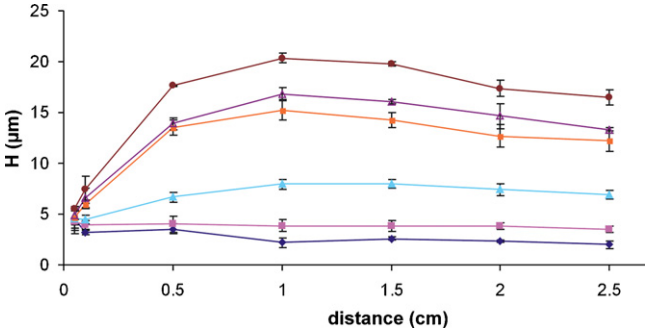


**Fig. 7.** Influence of the injection volume on the plate height evolution in the channel based on the experiments shown in Fig. 6. The sample had a viscosity contrast of 0.314 cP and the mobile phase velocity equalled $u = 2$ mm/s, while the injected peak volumes varied from 3.0 nl (—◆—), 9.0 nl (—●—), 14.1 nl (—▲—), 23.7 nl (—■—), 29.4 nl (—△—) to 32.7 nl (—●—).

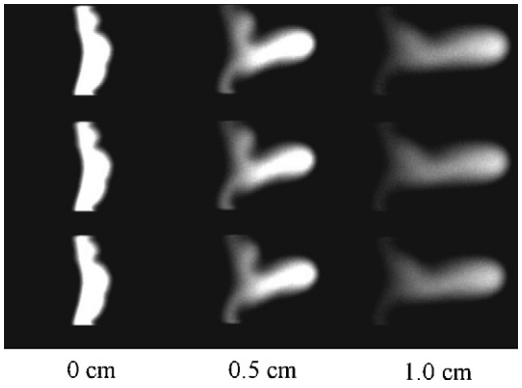


**Fig. 8.** Camera frames of consecutive injections of coumarin C480 (1 mM in methanol) in a mobile phase with a viscosity contrast of 0.314 cP (see also Fig. 5), monitored at the injection zone, at 0.5 cm and 1.0 cm.

downstream the bed inlet on, the finger also occupies about one half of the channel width, in agreement with the observations of Saffman [2] and also with a direct time-dependent analytical solution of the dispersion problem [35].

As already mentioned, the observed VF patterns were highly repeatable, even the asymmetrical start of the finger that is most prominent in the frame at a distance of 0.5 cm downstream of the bed inlet. As an example to corroborate this statement, Fig. 8 shows a succession of identical injections for the case of 0.314 cP viscosity contrast. A similar degree of reproducibility was observed for the other considered conditions. A moderating remark here is that the channel was only 3 cm long, so that we cannot exclude that in a longer channel more variability can be encountered. For low Reynolds numbers however, a high degree of reproducibility was observed in packed columns by Shalliker et al. [13]. Similarly, it might also be possible that at higher mobile phase velocities the behaviour becomes irreproducible. This was observed by the same authors [13].

In Fig. 9, the influence of the sign of the viscosity contrast is compared. In their numerical studies of VF effects for miscible slices, De Wit and co-workers have predicted different peak broadening behaviour when the contrast is inverted [36]. The fact that the case wherein the sample plug has a higher viscosity than the surrounding medium yields a lower dispersion (i.e., in the region >0.5 cm) than the opposite case is in qualitative agreement with their observations. Close to the bed inlet, however, the situation is reversed.

As a final moderating remark, it should also be noted that the bands will experience less VF-dispersion under retained conditions [25,11] than under the presently considered non-retained conditions, because the original medium into which the sample is dissolved moves faster than the analytes so that the latter are less influenced by the finger effect to which the original sample plug is subjected. However, this is especially true in reversed-phase or normal phase separations; and only to a lesser extent in applications such as SEC, where the analytes all elute relatively close to (or even with) the non-retained peak.

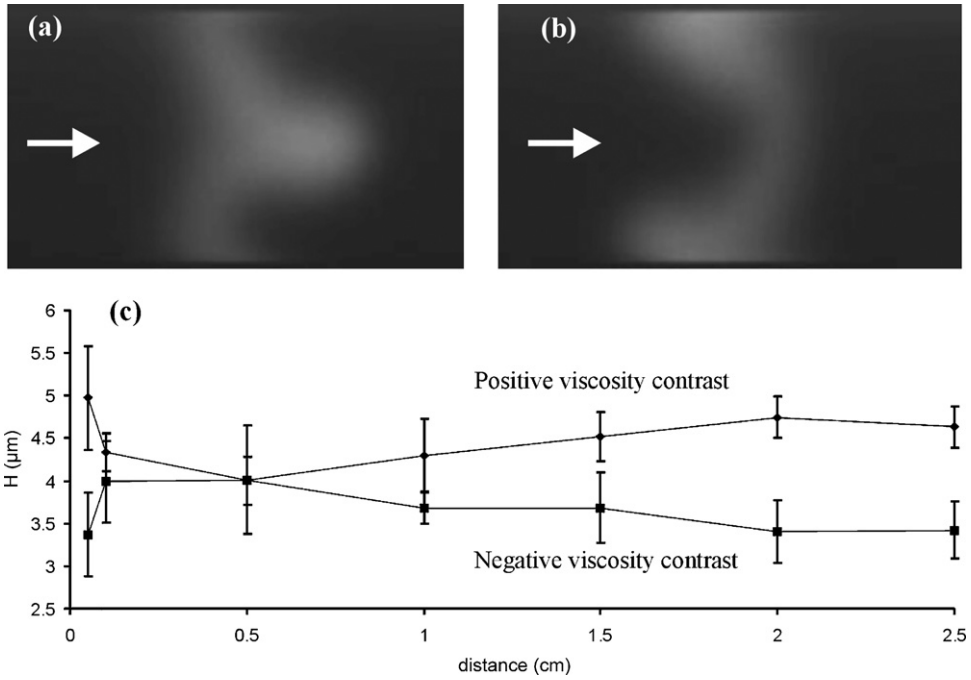


**Fig. 9.** (a) Camera image of a coumarin C480 band dissolved in pure methanol at 1 cm downstream the channel, with as mobile phase 10% water and 90% methanol (the flow direction is indicated by the white arrow), corresponding with a positive viscosity contrast ($\Delta\nu = 0.314$ cP), (b) camera image for a coumarin band dissolved in 10% water and 90% methanol at 1 cm in the channel with as mobile phase 100% methanol, corresponding with a negative viscosity contrast ($\Delta\nu = -0.314$ cP), to a situation where the fingering effect occurs at the upstream interface and (c) plate height evolution of cases (a) and (b) at several positions in the channel.

## 4. Conclusions

New experimental data of the viscous fingering (VF) process could be generated by studying the VF process in perfectly ordered pillar array columns instead of in the traditionally employed packed bed columns. A detailed quantitative analysis of the contribution of VF to the observed band broadening could be made by following the injected species bands using a fluorescence microscope equipped with a CCD-camera. The collected data form an ideal test set to be used to validate the ongoing theoretical modelling work, and will as such certainly contribute to a further understanding of this interesting phenomenon.

In agreement with theory, we could not observe a significantly measurable sudden threshold for the onset of VF, as the observed plate height values grew slowly but steadily with increasing viscosity contrast between the injected band and the mobile phase. The VF effect can be very significant (especially compared to the low plate heights that can be realized in high performance columns such as sub-2 μm particle columns or the presently employed pillar array columns): for a viscosity contrast of 0.16 cP, a plate height increase of about 1 μm can be observed, while for a contrast of respectively 0.5 cP and 1 cP, additional plate height contributions of the order of 5–20 μm were observed. Citing these values is however futile without noting that they also depend extremely strongly on the injection volume of injected sample. It was found that, for a given viscosity contrast of 0.314 cP, the maximal plate height increase varied between 0.5 μm and 18 μm if the injection volume was varied between 3.0 nl and 32.7 nl.

The observed VF patterns were highly repeatable. Given the highly ordered bed wherein the experiments were conducted, it can be assumed that the fingers were not induced by any local bed heterogeneities (a detailed SEM inspection did not reveal any visible bed defects). Instead, the formed finger patterns displayed a high degree of symmetry with respect to the bed cross-section, with one central finger formed at low viscosity contrast and three fingers (one large central one and two smaller, symmetrical positioned side-fingers) at high viscosity contrast.

The plate height values associated with the VF process also undergo a strong transient along the column length, first going through a steep increase (in the first few millimetre of the bed), then going through an optimum and finally gradually decreasing along the rest of the bed, as a consequence of ongoing sample dilution which gradually removes the viscosity contrast (and hence the VF contribution) completely. The relative extent to which VF may arise during a separation might hence strongly depend on the length of the column, with shorter columns being more prone to VF-induced dispersion than longer ones.

This dependency, together with the strong dependency on the injection volume, certainly complicates any quantitative VF analysis and prevents the direct comparison of different literature studies.

## References

[1] J.C. Moore, J. Sep. Sci. 5 (1976) 723.
[2] P.G. Saffman, G. Taylor, Proc. Roy. Soc. Lond. Ser. A (1958) 312.
[3] R.A. Shalliker, G. Guiochon, J. Chromatogr. A 1216 (2009) 787.
[4] G.M. Homsy, Ann. Rev. Fluid Mech. 19 (1987) 271.
[5] Y.C. Yortsos, J. Phys. Condens. Matter 2 (1990), SA 443.
[6] G. Rousseaux, A. De Wit, M. Martin, J. Chromatogr. A 1149 (2007) 254.
[7] E.J. Fernandez, C.A. Grotegut, G.W. Braun, K.J. Kirschner, J.R. Staudaher, M.L. Dickson, V. Fernandez, Phys. Fluids 7 (1995) 468.
[8] T.L. Ng, S. Ng, J. Chromatogr. 329 (1985) 13.
[9] M. Zapata, J.L. Garrido, Chromatographia 31 (1991) 589.
[10] C.B. Castell, R.C. Castells, J. Chromatogr. A 805 (1998) 55.
[11] K.J. Mayfield, R.A. Shalliker, H.J. Catchpoole, A.P. Sweeney, V. Wong, G. Guiochon, J. Chromatogr. A 1080 (2005) 124.
[12] R.A. Shalliker, H.J. Catchpoole, G.R. Dennis, G. Guiochon, J. Chromatogr. A 1142 (2007) 48.
[13] R.A. Shalliker, V. Wong, G. Guiochon, J. Chromatogr. A 1161 (2007) 121.
[14] D.E. Smith, X.Z. Wu, A. Libchaber, E. Moses, T. Witten, Phys. Rev. A 45 (1992) R2165.
[15] E.J. Fernandez, T.T. Norton, W.C. Jung, J.G. Tsavalas, Biotechnol. Prog. 12 (1996) 480.
[16] D. Cherrak, E. Guernet, P. Cardot, C. Herrenknecht, M. Czok, Chromatographia 46 (1997) 647.
[17] L.D. Plante, P.R. Romano, E.J. Fernandez, Chem. Eng. Sci. 49 (1994) 2229.
[18] M.L. Dickson, T.T. Norton, E.J. Fernandez, AIChE J. 43 (1997) 409.
[19] H.J. Catchpoole, R.A. Shalliker, G.R. Dennis, G. Guiochon, J. Chromatogr. A 1117 (2006) 137.
[20] D. Schafroth, N. Goyal, E. Meiburg, Eur. J. Mech. B/Fluids 26 (2007) 444.
[21] N. Goyal, E. Meiburg, J. Fluid. Mech. 558 (2006) 329.
[22] A.M. Rogerson, E. Meiburg, Phys. Fluids 17 (2005) 5.
[23] C.T. Tan, G. Homsy, Phys. Fluids 29 (1986) 3549.
[24] A. De Wit, Y. Bertho, M. Martin, Phys. Fluids 17 (2005) 054114.
[25] M. Mishra, M. Martin, A. De Wit, Phys. Fluids 19 (2007) 073101.
[26] G. Guiochon, N. Marchetti, K. Mriziq, R.A. Shalliker, J. Chromatogr. A 1189 (2008) 109.
[27] W. De Malsche, H. Eghbali, D. Clicq, J. Vangelooven, H. Gardeniers, G. Desmet, Anal. Chem. 79 (2007) 5915.
[28] W. De Malsche, H. Gardeniers, G. Desmet, Anal. Chem. 80 (2008) 5391.
[29] J. Vangelooven, W. De Malsche, H. Eghbali, K. Broeckhoven, H. Gardeniers, G. Desmet, Presented at the 29th International Symposium on Capillary Chromatography, Riva del Garda, Italy, May 25–30, 2007.
[30] J. Li, P.W. Carr, Anal. Chem. 69 (1997) 2530.
[31] J. Billen, K. Broeckhoven, A. Lievens, K. Choikhet, G. Rozing, G. Desmet, J. Chromatogr. A 1210 (2008) 30.
[32] N. Vervoort, J. Billen, P. Gzil, G.V. Baron, G. Desmet, Anal. Chem. 76 (2004) 4501.
[33] K. Broeckhoven, G. Desmet, J. Chromatogr. A 1172 (2007) 25.
[34] H. Eghbali, W. De Malsche, J. Desmet, J. Billen, M. De Pra, W.T. Kok, P.J. Schoenmakers, H. Gardeniers, G. Desmet, J. Sep. Sci. 30 (2007) 2605.
[35] M. Mineev-Weinstein, Phys. Rev. Lett. 80 (1998) 2113.
[36] M. Mishra, M. Martin, A. De Wit, Phys. Rev. E 78 (2008) 066306.